CHAPTER 7

RESULTS AND DISCUSSION

7.1 Analytical Study

The potential difference can be obtained through solid state thermionic conversion, i.e. heat to electricity, for various materials of high work function at different temperatures, as shown in Fig 7.1, after simulation of mathematical equation prepared on Labview using both Richardson Dushman Equation and Child's law.

The potential difference values produced by thermionic conversion of heat energy for coating materials with low work function at different temperatures are also included in the results, as shown in Fig 7.2, and both are displayed in graphical form for comparison.

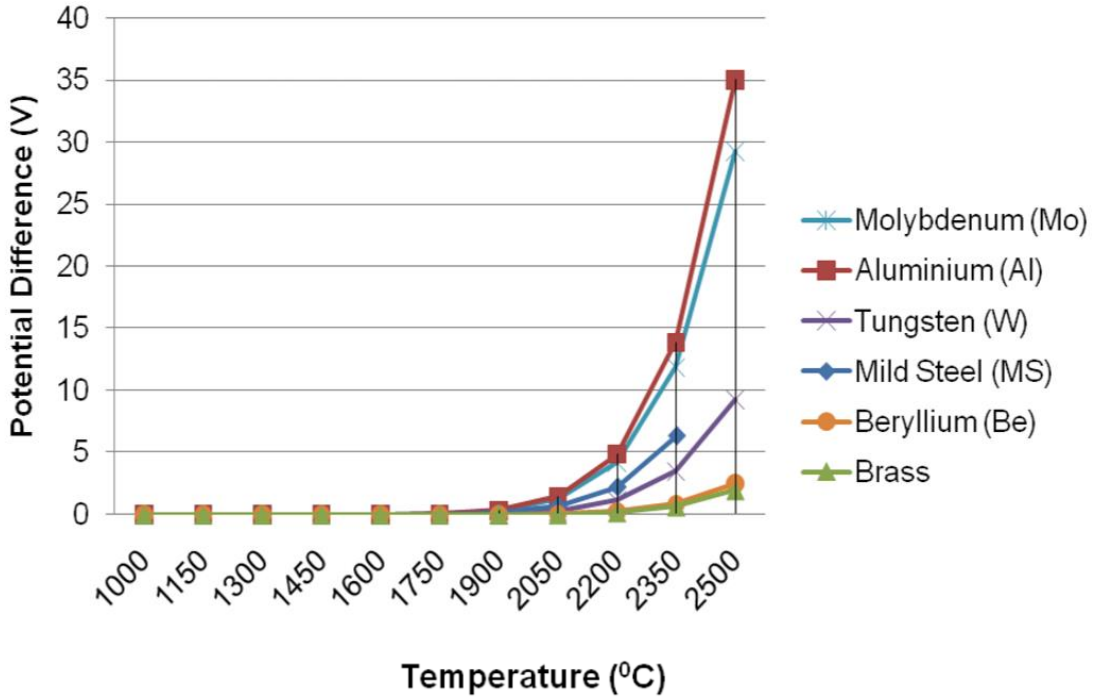

Fig. 7.1. Effect of Temperature on Potential Difference between Emitter and Collector (Without Coating) collector *(Source: Appendix I Data)*

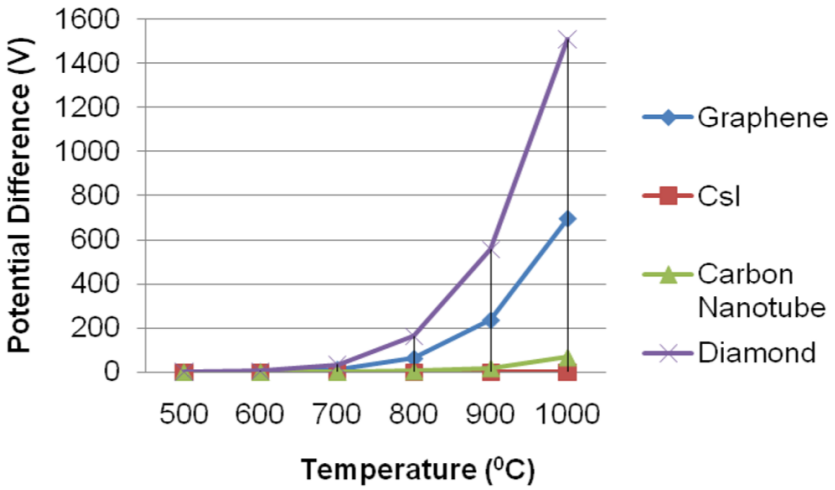

Fig. 7.2. Effect of Temperature on Potential Difference between Emitter and Collector (With Coating) collector *(Source: Appendix II Data)*

7.1.1 Discussion on results of analytical study

The above-mentioned analytical study is required for informing the thermionic emission and direct energy conversion. Material selection is a crucial part of this research since a thorough examination of materials has revealed that reduced work function material coatings can increase TEC performance. The results show that the preceding assertion is true, since they show a comparison of different materials with varied values of different work-functions at various temperatures. It can be seen that the quantity of potential difference obtained increases when the work function is reduced and the temperature is increased.

Figure 7.1 shows that even at higher temperatures, such as 2500^0C, which is significantly higher than its melting point, the material Brass with the highest work-function is unable to execute the predicted thermionic conversion of heat into electricity. At temperatures exceeding 1800^0C, molybdenum and tungsten with lesser work functions show a greater potential difference.

Aluminium is the best material for thermionic emission, according to the studies, but its melting point is substantially lower than the temperature at which it will emit electrons. Mild steel and beryllium have substantially lower work functions than brass, yet the results demonstrate that Beryllium emits similar emissions to brass, while Mild steel has a higher potential difference. However, these two metals share the same issue as brass and aluminium, namely, a lower melting point.

Figure 7.2 shows a similar situation. Two other materials with lower work-functions, such as CsI, Carbon nanotube, Graphene, and diamond, are compared. At an extremely low operating temperature, 700^0C, the ultralow work-function of diamond acquired a greater potential difference. In comparison to typical metals, graphene has showed a considerable difference in potential at very low temperatures.

Although the potential difference between carbon nanotubes and CsI (Caesium iodide) coating is less than that between graphene and diamond, the results are significant and effective. As a result of the findings, it can be concluded that all materials, with the exception of Tungsten and Molybdenum, have melting points lower than the Thermionic emission temperature. As a result, a low work function material coating is required over materials that emit at a lower temperature, i.e. 900^0C.

An engine's waste heat recovery requires a Heat Balance Sheet to calculate the heat supplied and heat lost. The integrated circuit (IC) engine The heat calculation used in the analytical study reveals that using an engine diagnostics tool, real-time fuel consumption data may be produced. Heat loss in cooling and exhaust can also be calculated using temperature data from the exhaust and cooling systems. The results in Figures 7.3, 7.4, and 7.5 show that a virtual simulation of the Richardson Equation and Child's rule for mathematical thermionic emission is the optimum way for understanding any material's behaviour. The software analysis is carried out with the help of LabVIEW. This also demonstrates how an analytical analysis simplifies the selection of materials and design standards for TEC.

A. Electric potential profile

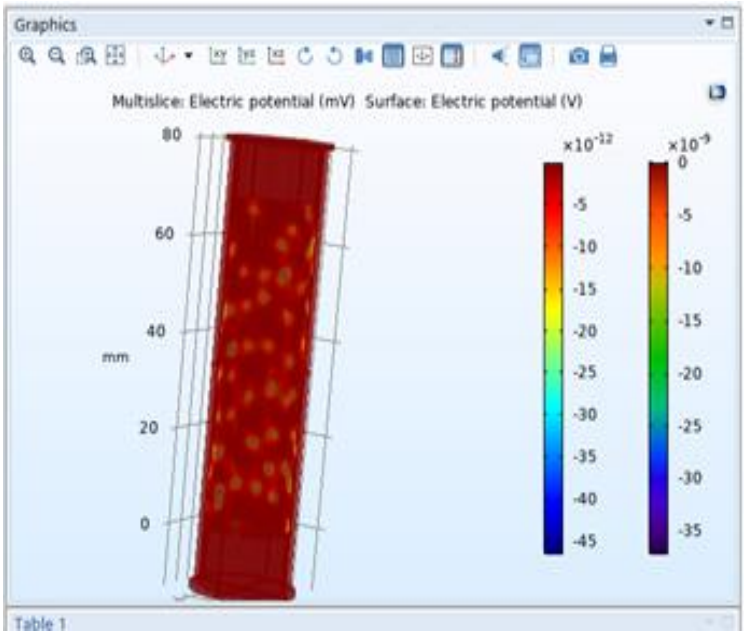

Fig. 7.3. Electric Potential between Emitter and Collector

B. Particle Trajectories

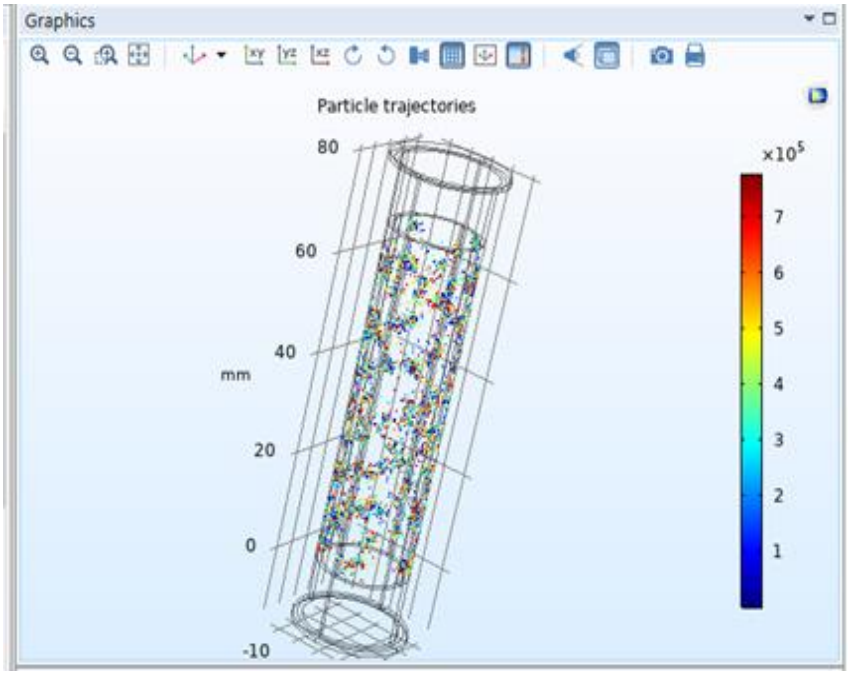

Fig. 7.4. Particle Trajectories Showing Thermionic Emission

C. Electric Potential

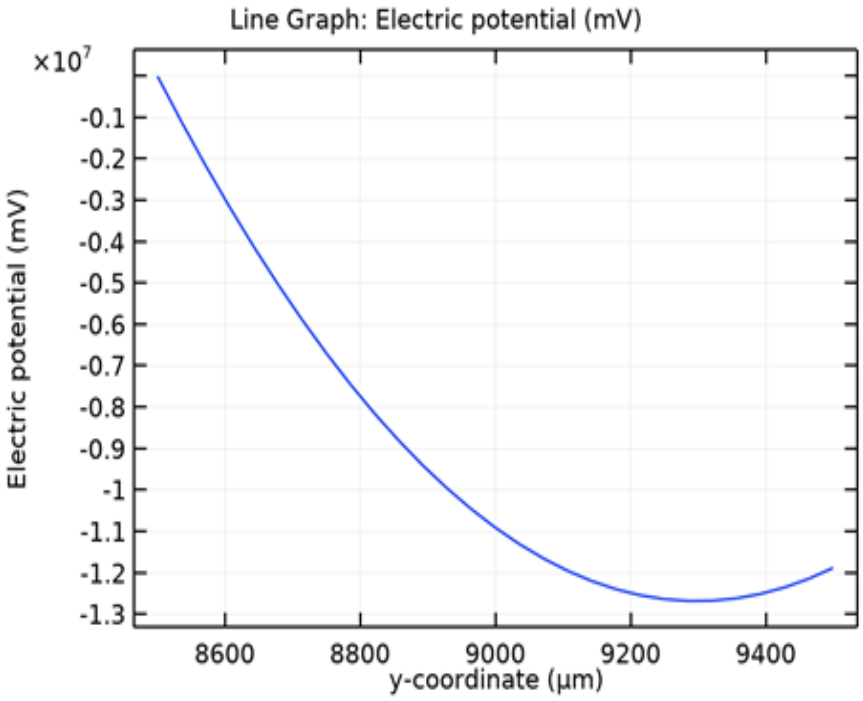

Fig. 7.5. Electric Potential in Emitter to Collector Region

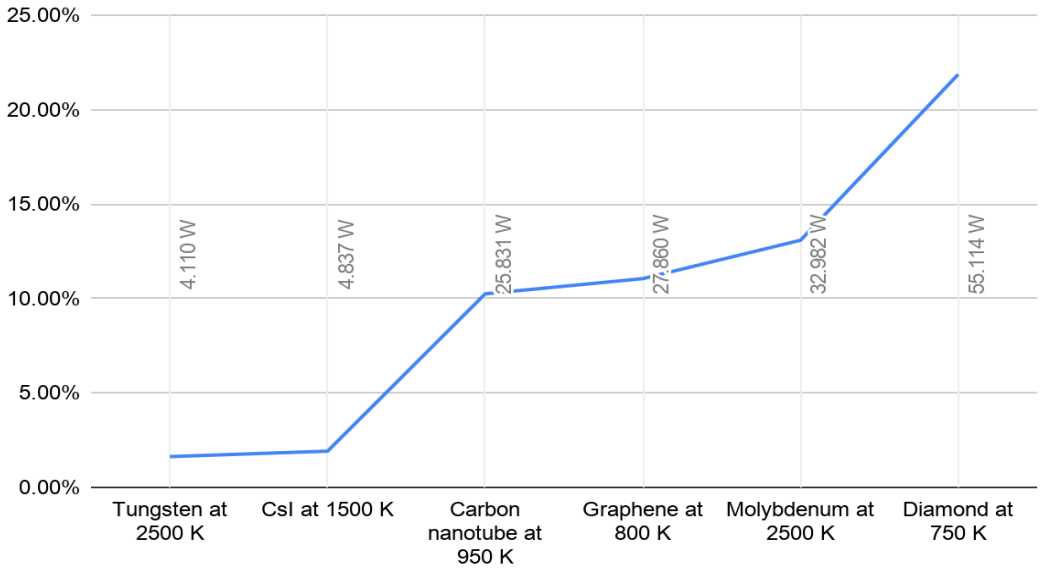

Fig. 7.6. Graph of Power output and Efficiencies *(Source: Appendix III Data)*

The results are the outcome of mathematical expressions for thermionic emission and the 3D design of thermionic energy converters. Power output and efficiency measurement of thermionic energy converter based on Richardson-Dushman equation are shown in Fig. 7.6.

The voltage outputs of materials are taken from electric potential profile. The current density values and electric potential considered for calculating power output. Diamond and Graphene showing better conversion efficiencies with higher electric output stands best as emitter and collector materials. The graph showing electric potential between electrodes is a profile of electron trajectory as discussed in the conceptual model earlier. It is evident from particle trajectories and electric potential graph that thermionic emission is occurring in the design.

Voltage vs. Temperature plots (Data sheets are attached in Appendix);

1) Comparison of simulation and experimental data for Aluminium emitter

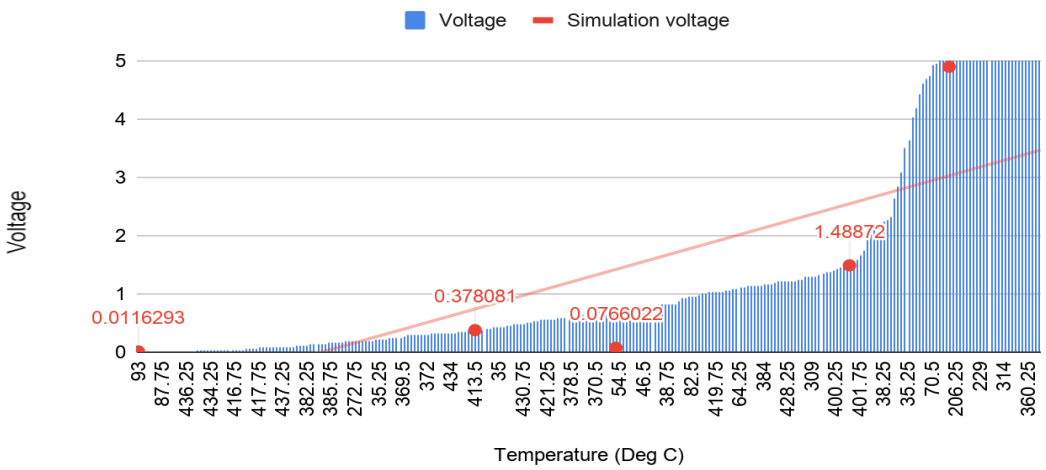

Fig. 7.7. Results for Aluminium as Emitter and Molybdenum as a Collector *(Source: Appendix IV Data)*

Simulation data

Experimental data

2) Comparison of simulation and experimental data for Brass emitter

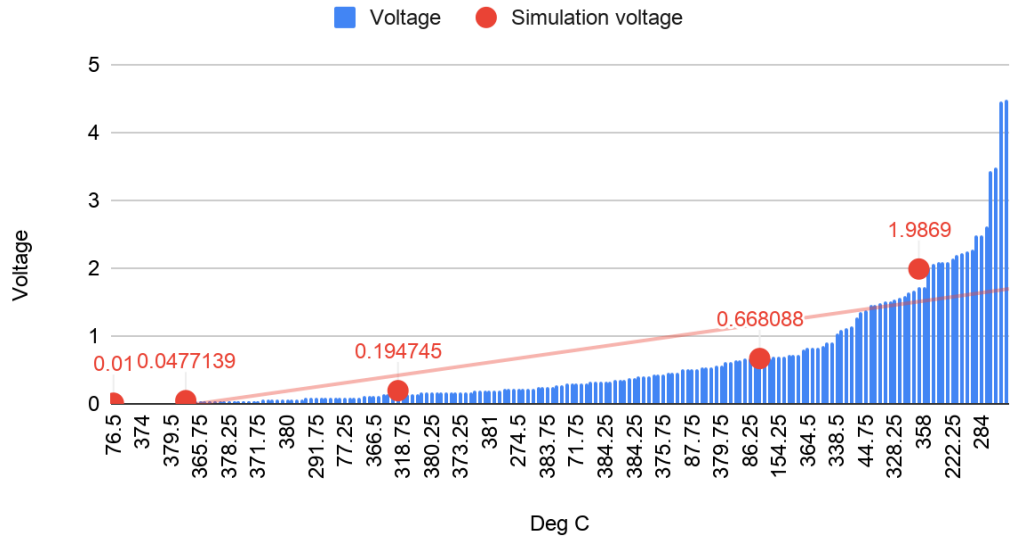

Fig. 7.8. Results for Brass as emitter and Molybdenum as a collector *(Source: Appendix V Data)*

3) Comparison of simulation and experimental data for Mild steel emitter

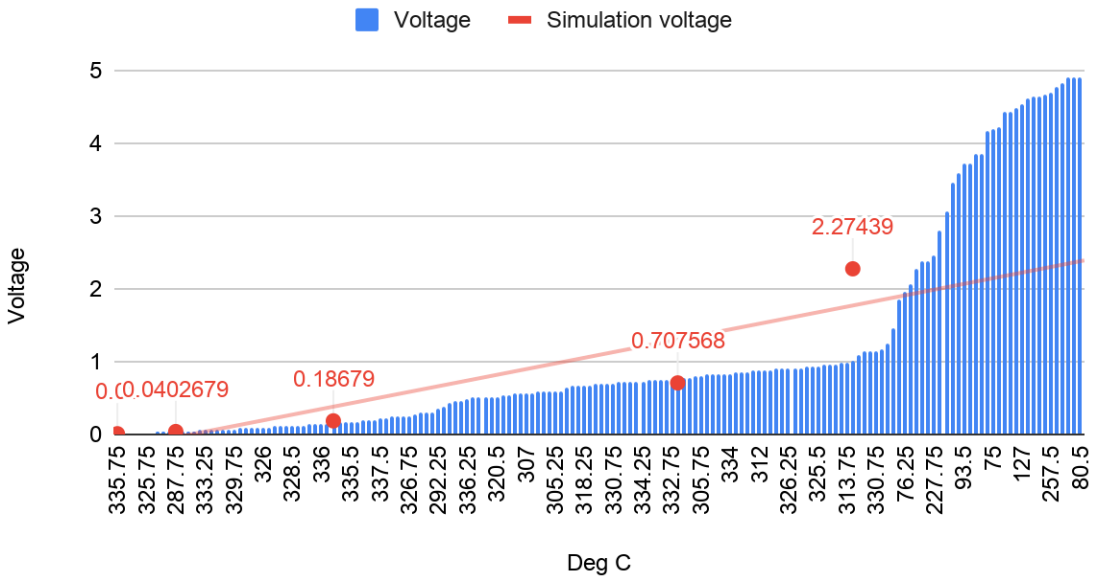

Fig. 7.9. Results for Mild Steel as emitter and Molybdenum as a collector *(Source: Appendix VI Data)*

The above plots in Fig. 7.7, Fig. 7.8 & Fig. 7.9 are the output from prototype thermionic energy convertor when tested for different available materials at temperatures up to 430^0C. In the experiment maximum temperature for Mild Steel, Aluminium & Brass emitter was kept 430^0 C because no significant output was achieved. Also the melting point for Aluminium is low therefore there were chances of deformation. The output voltages are DC voltages but no constant voltage was observed. It is also evident from the analytical and simulation study that the metal which were tested experimentally are not sufficient to generate higher potential difference.

The developed LabVIEW and COMSOL Multiphysics modules were simulated by varying material properties and temperature inputs. Experiment is conducted on prototype test setup using tungsten and molybdenum electrodes. The results obtained from simulations and experimentation are discussed below;

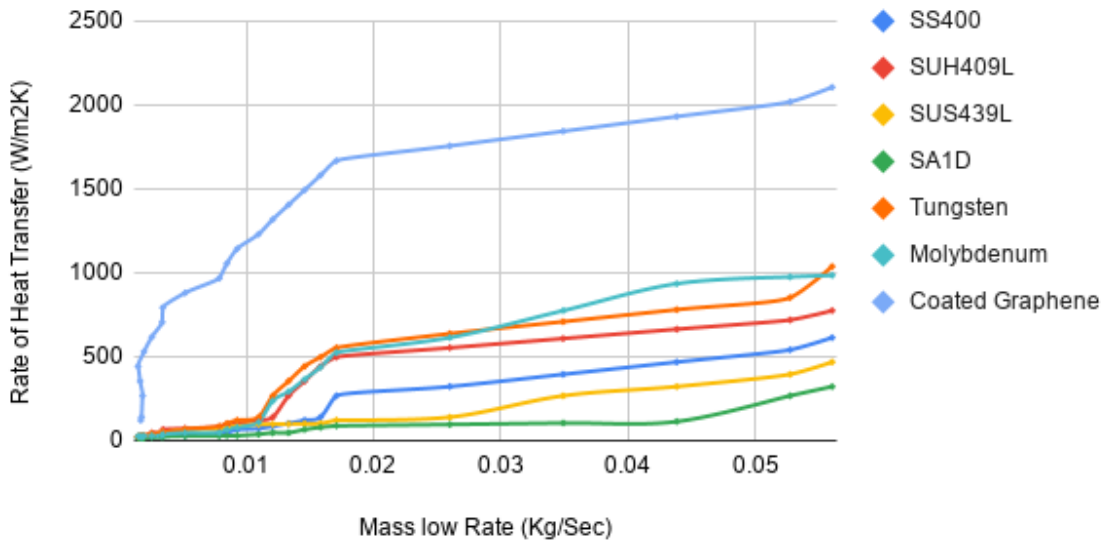

Fig. 7.10. Heat Transfer Analysis *(Source: Appendix VII Data)*

The Fig. 7.10 shows proportional relation between rate of heat transfer and exhaust gas mass flow rate. The graphene shows highest heat flux of 2107.09 W/m^{2}K in comparison with other materials. SA1D has lowest heat transfer rate of 322.46 W/m^{2}K. Tungsten and molybdenum have relatively higher heat flux of 1038.73 W/m^{2}K and 985.43 W/m2K. More the heat transferred more will be the thermionic emission. It can be concluded that the tungsten and molybdenum as an exhaust pipe materials can improve the thermionic conversion with higher thermionic emission. (Data sheet is attached in Appendix)

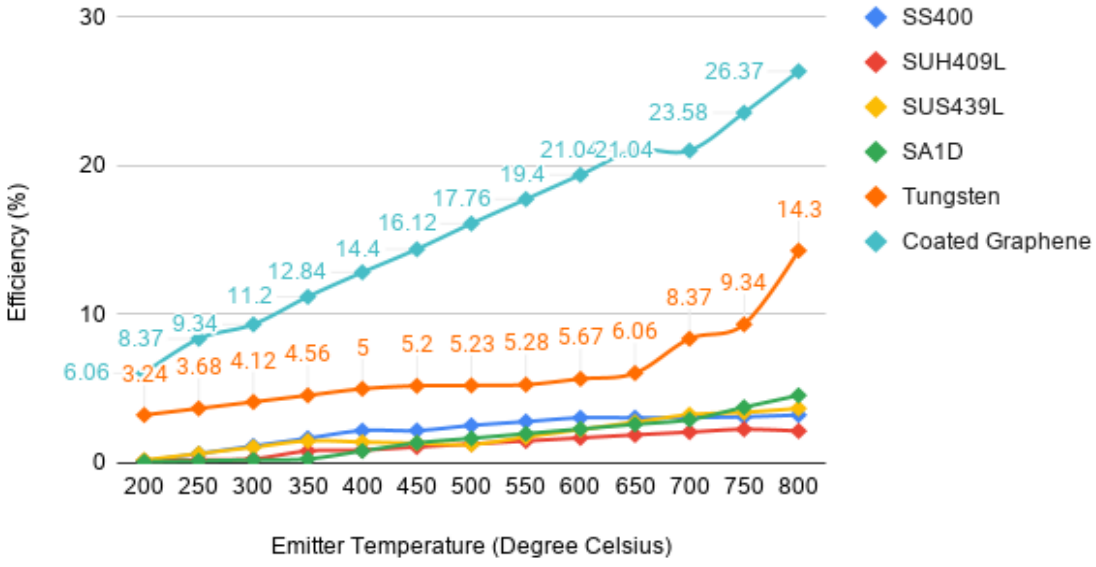

Fig. 7.11. Thermionic Emission Analysis *(Source: Appendix VII Data)*

The LabVIEW modules were used to get heat transfer and conversion efficiencies of materials considered. The graph in Figure 7.11 shows results obtained from the modules for conversion efficiencies of pipe materials with variation in temperature. Highest conversion efficiency of 26.37% is obtained from graphene coatings whereas significant conversion of 14.3% is obtained from tungsten emitter. (Data sheets are attached in Appendix)

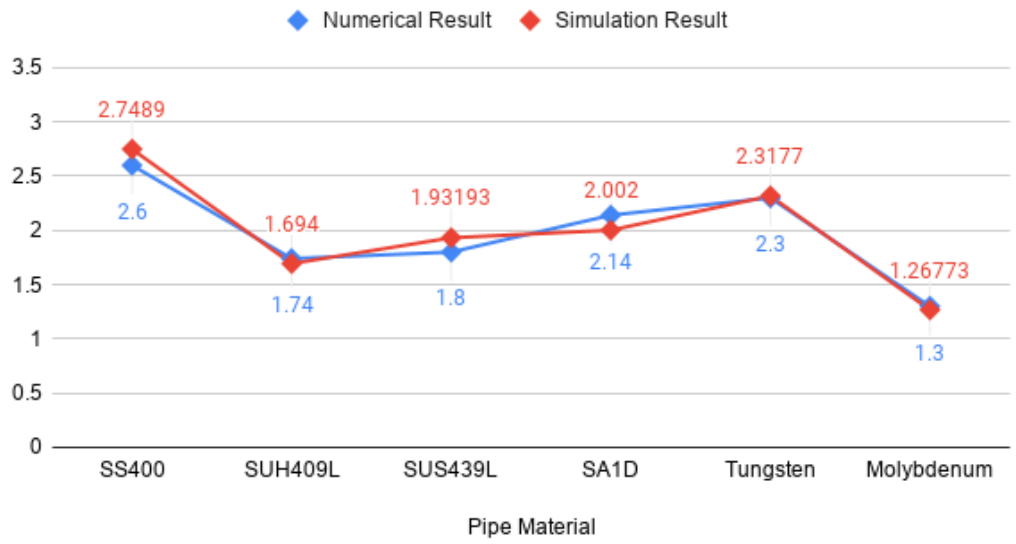

Fig. 7.12. Thermal Stress Analysis *(Source: Appendix VIII Data)*

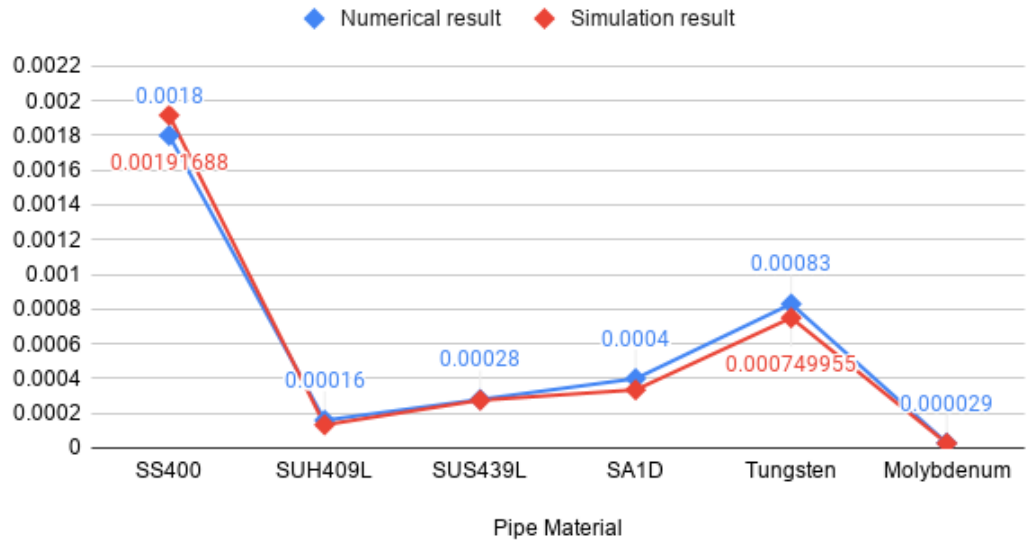

Fig. 7.13. Thermal Strain Analysis *(Source: Appendix VIII Data)*

The thermal stress strain analysis results are shown in Figure 7.12 and Fig.7.13. The thermal stress and strain developed in tungsten and molybdenum are similar in comparison with other existing exhaust pipe materials. Hence, it can be considered from

this analysis that tungsten and molybdenum as exhaust pipe material can sustain the thermal load.

Simulation vs. experimentation results

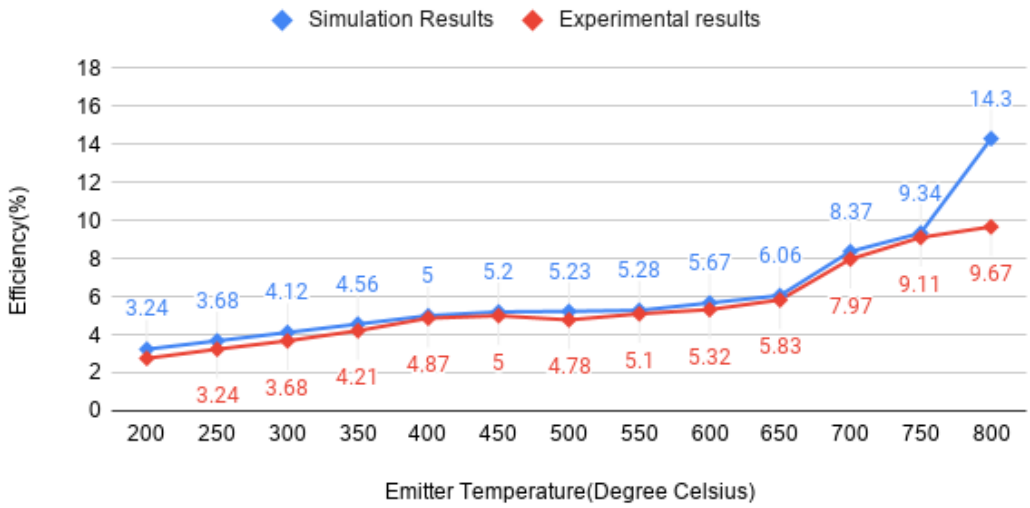

Fig. 7.14. Experimentation Result *(Source: Appendix IX Data)*

The experiments were performed on prototype test setup with tungsten as emitter and molybdenum as collector. Fig. 7.14 shows thermionic conversion results obtained from the experiments. The experimental results are compared with simulation results obtained from COMSOL multiphysics module.

The graph shows that experimental results follow simulation path till 750^0 C with a marginal error. Whereas a relative error of 32.377% is recorded at 800^0C. The error was observed as simulation is done by considering ideal conditions whereas experimental setup has limitations in DAQ tool & cartridge heater maximum limit was 800^0C.

7.2. MATLAB simulation

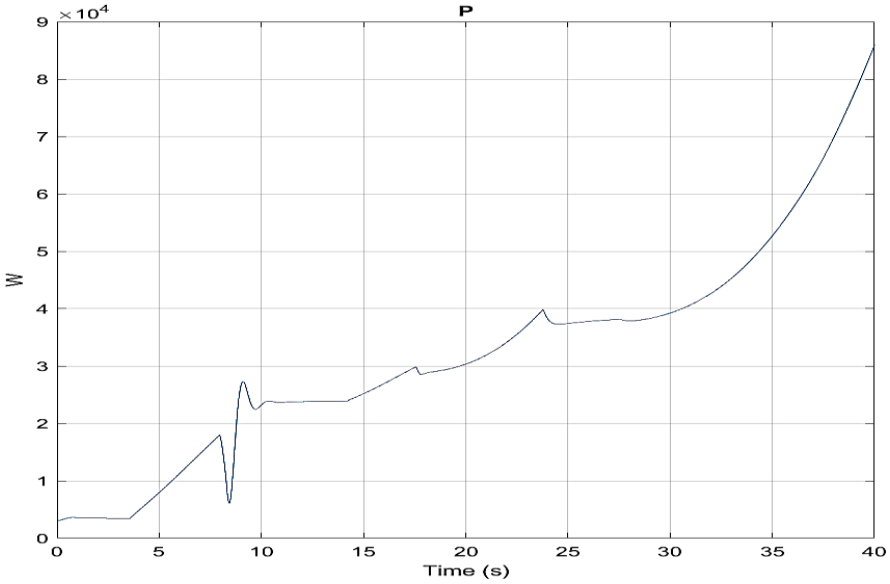

Fig. 7.15. Engine Power Source: (*Spark-Ignition Engine from Intake to Exhaust Port - Simulink - MathWorks India*, n.d.)

The Fig. 7.15 shows the engine power versus time curve. The engine maximum power output of 85 KW is achieved.

7.3. Fuel Consumption without TRS

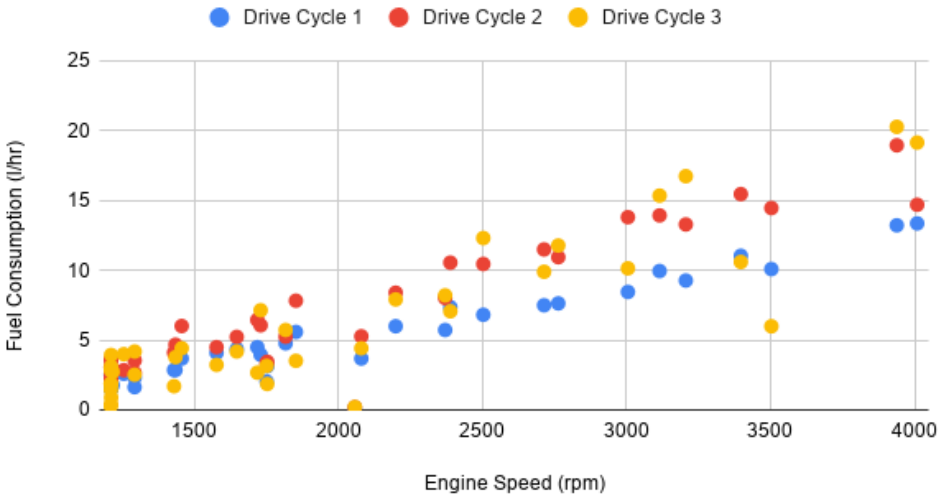

Fig. 7.16. Fuel Consumption without TRS *(Source: Appendix I Data)*

7.4. Fuel Consumption with TRS

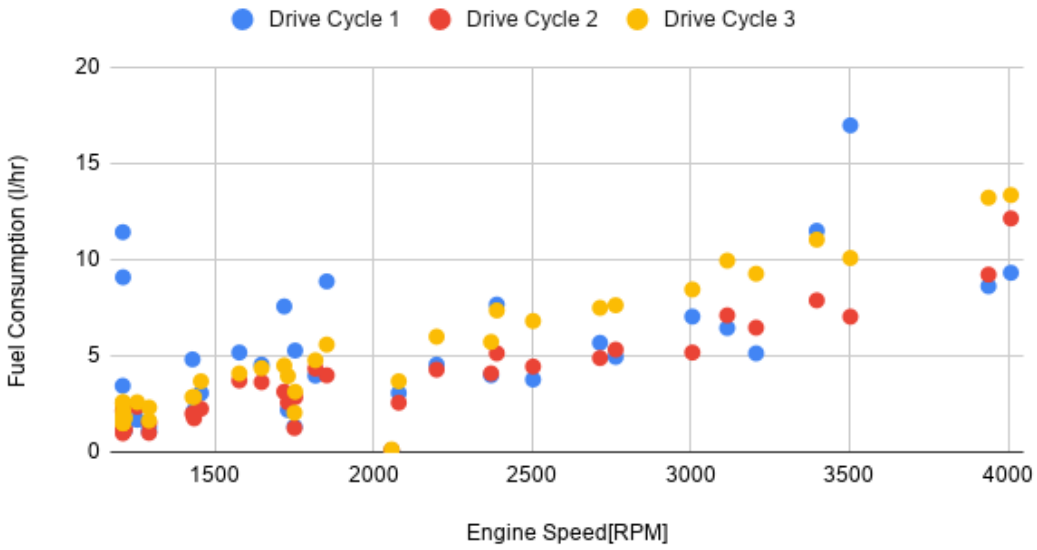

Fig. 7.17. Fuel Consumption with TRS *(Source: Appendix Data)*

The graphs shown in Fig. 7.16 & Fig. 7.17. Represent the fuel consumption data collected from the simulation of hybrid electric vehicle model in Simulink matlab. The maximum fuel consumption without TRS of Drive cycle 1 is 14 l/hr, drive cycle 2 is 18 l/hr, and drive cycle 3 is 20 l/hr.

Whereas the maximum fuel consumption with TRS of Drive cycle 1 is 12.5 l/hr, drive cycle 2 is 12 l/hr, drive cycle 3 is 13 l/hr. The fuel consumption is reduced in all drive cycles and the Drive cycle 3 is showing maximum 23% reduction in fuel consumption with use of TRS in a HEV.

7.5. TRS Power Output

As shown in Fig. 7.18, during urban driving cycle a maximum 6KW of power output from TRS after 120sec running time for drive cycle 1, 200 sec running time for drive cycle 2 &3. It can be stated that the thermionic regeneration system starts working with its maximum & constant output after 120-200 Sec depending upon vehicle operation. From the above results it is found that a TRS model having tungsten and molybdenum as emitter and collector respectively have a significant electrical power output.

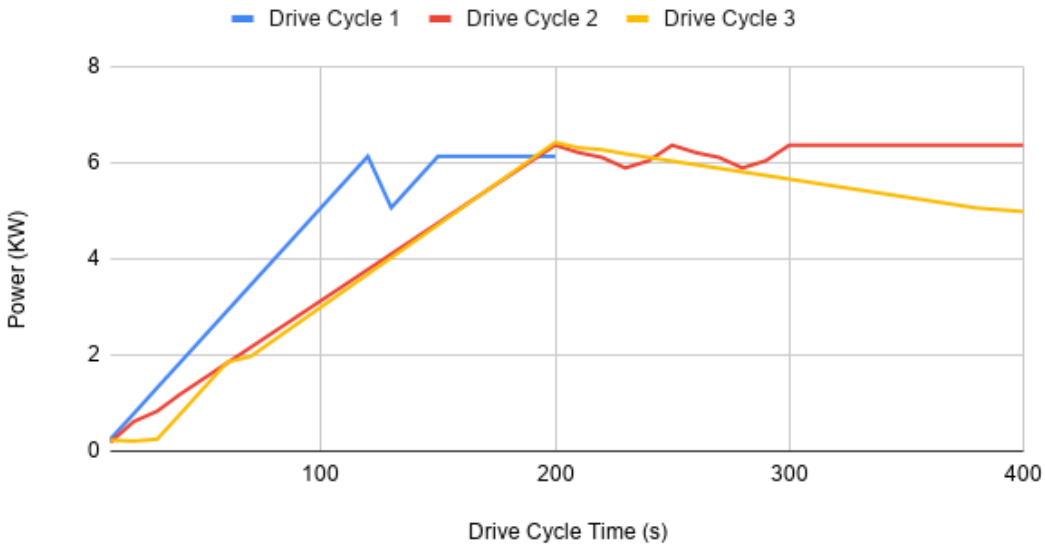

Fig. 7.18. TRS Output power *(Source: Appendix I Data)*

7.6. Validation

In this research, the validation of design is performed with a thermionic emission module using design simulation on COMSOL multiphysics software. The thermionic emission module is based on Richardson dushman equation. The results of design simulation have validated that there is an electrical insulation and potential difference generation as shown in Fig. 7.5. The design is verified after manufacturing with electric continuity and voltage measurements.

The simulation and experimentation results from Fig. 7.14 shows experimental values followed the simulation path, except at 800^0C were the cartridge heater limit was achieved. The result also verifies the mathematical model developed for simulation.

The integration of TRS with HEV models is validated with the control algorithm run, results are shown in Fig. 7.15. The achieved conversion efficiency of 14.3% is higher in comparison with current research based on thermoelectric devices i.e. 5.7% (which are still under research). (Fairbanks, n.d.)

7.7. Limitation

Material Selected for experimentation is limited to tungsten and molybdenum instead of coated graphene/ caesium due to availability of resources and machining methodologies. Full Vehicle simulation is limited to Indian Driving Cycles. System model of TRS is integrated with existing HEV reference models.

The development stage is limited to full vehicle modelling and simulation instead of on vehicle testing, because of following reasons;

1) Availability of material & their manufacturing methods
2) Cost effectiveness
3) Time utilization
4) Unavailability of full hybrid electric vehicle